

Review Article

Basic Principles and Practical Applications of the Cahn–Hilliard Equation

Junseok Kim,¹ Seunggyu Lee,² Yongho Choi,¹ Seok-Min Lee,³ and Darae Jeong¹

¹Department of Mathematics, Korea University, Seoul 02841, Republic of Korea

²National Institute for Mathematical Sciences, Daejeon 34047, Republic of Korea

³Department of Liberal Arts, College of Engineering, Hongik University, 94 Wausan-ro, Mapo-gu, Seoul 04066, Republic of Korea

Correspondence should be addressed to Darae Jeong; tinayoyo@korea.ac.kr

Received 20 July 2016; Accepted 5 October 2016

Academic Editor: Qin Yuming

Copyright © 2016 Junseok Kim et al. This is an open access article distributed under the Creative Commons Attribution License, which permits unrestricted use, distribution, and reproduction in any medium, provided the original work is properly cited.

The celebrated Cahn–Hilliard (CH) equation was proposed to model the process of phase separation in binary alloys by Cahn and Hilliard. Since then the equation has been extended to a variety of chemical, physical, biological, and other engineering fields such as spinodal decomposition, diblock copolymer, image inpainting, multiphase fluid flows, microstructures with elastic inhomogeneity, tumor growth simulation, and topology optimization. Therefore, it is important to understand the basic mechanism of the CH equation in each modeling type. In this paper, we review the applications of the CH equation and describe the basic mechanism of each modeling type with helpful references and computational simulation results.

1. Introduction

The Cahn–Hilliard (CH) equation is a mathematical model of the process of a phase separation in a binary alloy [1, 2]. Its physical applications have been extended to many areas of scientific fields such as spinodal decomposition [1, 3], diblock copolymer [4–6], image inpainting [7], multiphase fluid flows [8–10], microstructures with elastic inhomogeneity [11, 12], tumor growth simulation [13, 14], and topology optimization [15, 16]. In this paper, we review and describe the basic mechanism of each model. The basic building-block equation of the mathematical modeling and dynamical model is the CH equation:

$$\begin{aligned} \frac{\partial \phi}{\partial t}(\mathbf{x}, t) &= \nabla \cdot [M(\phi(\mathbf{x}, t)) \nabla \mu(\mathbf{x}, t)], \quad \mathbf{x} \in \Omega, \quad t > 0, \\ \mu(\mathbf{x}, t) &= F'(\phi(\mathbf{x}, t)) - \epsilon^2 \Delta \phi(\mathbf{x}, t), \\ \frac{\partial \phi}{\partial n}(\mathbf{x}, t) &= \frac{\partial \mu}{\partial n}(\mathbf{x}, t) = 0, \quad \mathbf{x} \in \partial \Omega, \end{aligned} \quad (1)$$

where $\Omega \subset \mathbb{R}^d$ ($d = 1, 2, 3$) is a bounded domain with a boundary $\partial \Omega$. The quantity $\phi(\mathbf{x}, t) = m_\alpha - m_\beta$ is a phase-field defined as the difference between the mole fractions of binary mixtures, where m_α and m_β are the mole fractions of phases α and β . $F(\phi) = 0.25(\phi^2 - 1)^2$ is a double-well potential of a homogeneous system of composition ϕ as shown in Figure 1. $M(\phi(\mathbf{x}, t))$ is a positive mobility, ϵ is a positive constant, and $\partial/\partial n$ is the outward normal derivative at the domain boundary. Originally, the concentration-dependent mobility has a form $M(\phi) = M_0(1 - \phi)(1 + \phi)$, where M_0 is a constant. This form has the same property in diseases transmission in that transmission happens by contact.

The CH equation can be derived from the total free energy functional

$$\mathcal{E}(\phi) = \int_{\Omega} \left(F(\phi) + \frac{\epsilon^2}{2} |\nabla \phi|^2 \right) d\mathbf{x}. \quad (2)$$

Now, we get the chemical potential from (2): $\mu = \delta \mathcal{E}/\delta \phi = F'(\phi) - \epsilon^2 \Delta \phi$. Then, by the mass conservation, we have the CH

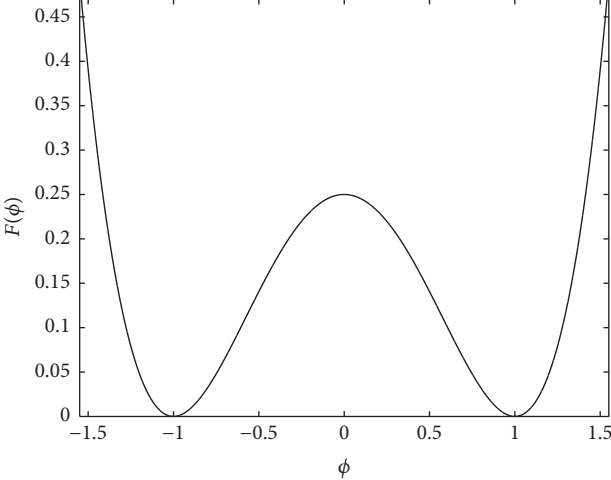


FIGURE 1: Double-well potential function $F(\phi) = 0.25(\phi^2 - 1)^2$.

equation: $\phi_t = -\nabla \cdot \mathcal{J}$, where the flux is defined as $\mathcal{J} = -M\nabla\mu$. The CH system (1) possesses the following two properties:

$$\begin{aligned} \frac{d}{dt} \int_{\Omega} \phi \, d\mathbf{x} &= 0, \\ \frac{d}{dt} \mathcal{E}(t) &\leq 0. \end{aligned} \quad (3)$$

See [18] for more details about the physical, mathematical, and numerical derivations of the binary Cahn–Hilliard equation.

The objective of this paper is to review the physical applications of the CH equation. This paper is organized as follows. In Section 2, we present spinodal decomposition of a binary alloy, which is the original application of the CH equation. By adding a long-range nonlocal energy, we have a mathematical model for the diblock copolymers in Section 3. A slightly modified CH equation is applied to the inpainting of binary images in Section 4. In Section 5, we present a two-phase immiscible fluid flow model which uses the CH equation to represent two distinct fluids. Elastic strain energy takes an important role in a solid-state phase transformation. When the free energy functional includes this additional effect, the microstructure evolution can be modeled using the CH equation. We consider this in Section 6. In Section 7, we review tumor growth model in which the CH equation accounts for the cell species. In Section 8, we consider structure optimization problem in which we need to minimize mean compliance of the multimaterial structures. Finally, conclusions are drawn in Section 9.

2. Spinodal Decomposition

A system of the CH equations (1) is the leading model of spinodal decomposition in binary alloys. Spinodal decomposition is a process by which a mixture of two materials can separate into distinct regions with different material concentrations [1]. Morphological patterns during spinodal decomposition

and subsequent coarsening for interface-diffusion-controlled dynamics are shown in Figure 2.

The simulation is performed on a two-dimensional domain $\Omega = (0, 1) \times (0, 1)$ with 128×128 mesh grid; that is, the spatial step size $h = 1/128$. The initial condition is given by $\phi(x, y) = \bar{\phi} + 0.05 \text{rand}(x, y)$, where $\bar{\phi}$ is an average value of $\phi(x, y)$ and $\text{rand}(x, y)$ is a random number function distributed uniformly in $[-1, 1]$. The temporal step size $\Delta t = h^2$ and $\epsilon = 0.0075$ are used. As shown in Figure 2, we can see two different patterns with respect to $\bar{\phi}$. The upper and lower rows in Figure 2 represent the time evolution of numerical results with $\bar{\phi} = -0.4$ and $\bar{\phi} = 0$, respectively. In these tests, we used the nonlinearly stabilized splitting scheme [19]. There are many other numerical methods [20–27] that can be applied to the CH equations.

3. Diblock Copolymer

A diblock copolymer is a linear-chain molecule consisting of two subchains joined covalently to each other [4]. Let $\phi(\mathbf{x}, t) = \rho_A(\mathbf{x}, t) - \rho_B(\mathbf{x}, t)$ be the order parameter which is defined as the difference between the local volume fractions of A and B monomers at point \mathbf{x} and time t . Then, the governing equation by the Ohta–Kawasaki model [28] is as follows:

$$\begin{aligned} \frac{\partial \phi(\mathbf{x}, t)}{\partial t} &= \Delta \left(F'(\phi(\mathbf{x}, t)) - \epsilon^2 \Delta \phi(\mathbf{x}, t) \right) \\ &\quad - \alpha (\phi(\mathbf{x}, t) - \bar{\phi}), \quad \mathbf{x} \in \Omega, \end{aligned} \quad (4)$$

where $\Omega \subset \mathbb{R}^d$ ($d = 1, 2, 3$) is a domain, $\bar{\phi} = \int_{\Omega} \phi \, d\mathbf{x}/|\Omega|$ is the spatial average of ϕ , and α is inversely proportional to the square of the total chain length of the copolymer [29]. Equation (4) can be derived from the following free energy functional:

$$\begin{aligned} \mathcal{E}(\phi) &= \int_{\Omega} \left(F(\phi(\mathbf{x})) + \frac{\epsilon^2}{2} |\nabla \phi(\mathbf{x})|^2 \right) d\mathbf{x} \\ &\quad + \frac{\alpha}{2} \iint_{\Omega} G(\mathbf{x}, \mathbf{y}) (\phi(\mathbf{x}) - \bar{\phi})(\phi(\mathbf{y}) - \bar{\phi}) \, d\mathbf{x} \, d\mathbf{y}, \end{aligned} \quad (5)$$

where $F(\phi) = 0.25(\phi^2 - 1)^2$ and $G(\mathbf{x}, \mathbf{y})$ denotes Green's function of $-\Delta$ on Ω with periodic boundary conditions [4].

As a test problem, we perform a numerical test with respect to $\bar{\phi}$ on the domain $\Omega = (0, L) \times (0, L)$. In this test, we set the initial condition as $\phi(x, y, 0) = \bar{\phi} + 0.1 \text{rand}(x, y)$, where $\text{rand}(x, y) \in [-1, 1]$ is a randomly generated number. The other parameters used are $h = 0.03$, $\Delta t = 0.1$, $\alpha = 100$, $\epsilon = 0.035$, $L = 128h$, and 128×128 mesh grid. Figures 3(a) and 3(b) show the evolution of the numerical solutions with $\bar{\phi} = -0.3$ and $\bar{\phi} = 0$, respectively. As shown in Figure 3(a), figures in the first row change to the hexagonal geometry as time increases. Unlike this, we can see the lamellar geometry in Figure 3(b) at the equilibrium state.

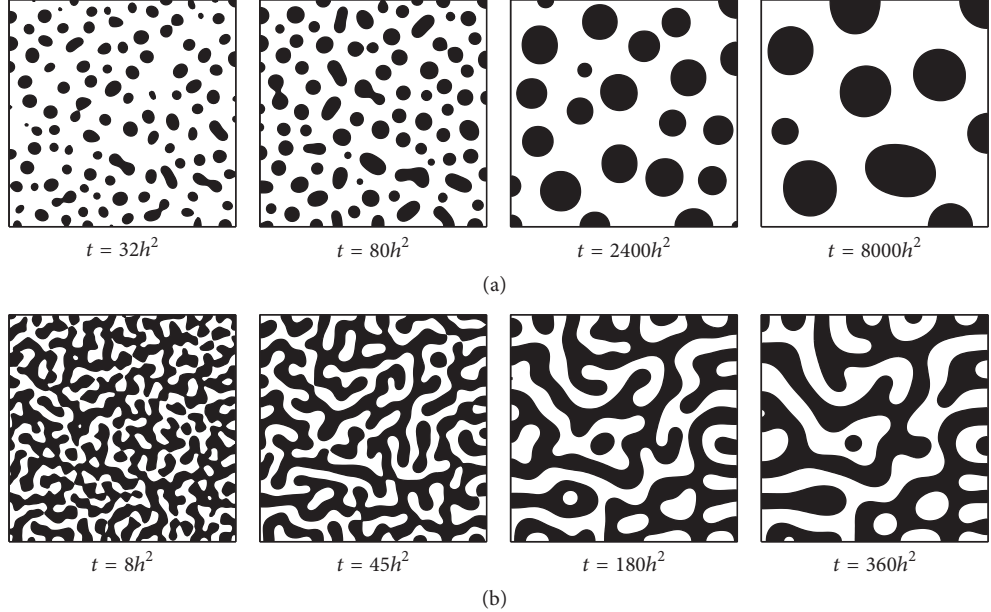


FIGURE 2: Morphological patterns during spinodal decomposition and subsequent coarsening. The upper and lower rows represent the results with (a) $\bar{\phi} = -0.4$ and (b) $\bar{\phi} = 0$, respectively. Times are shown below each figure.

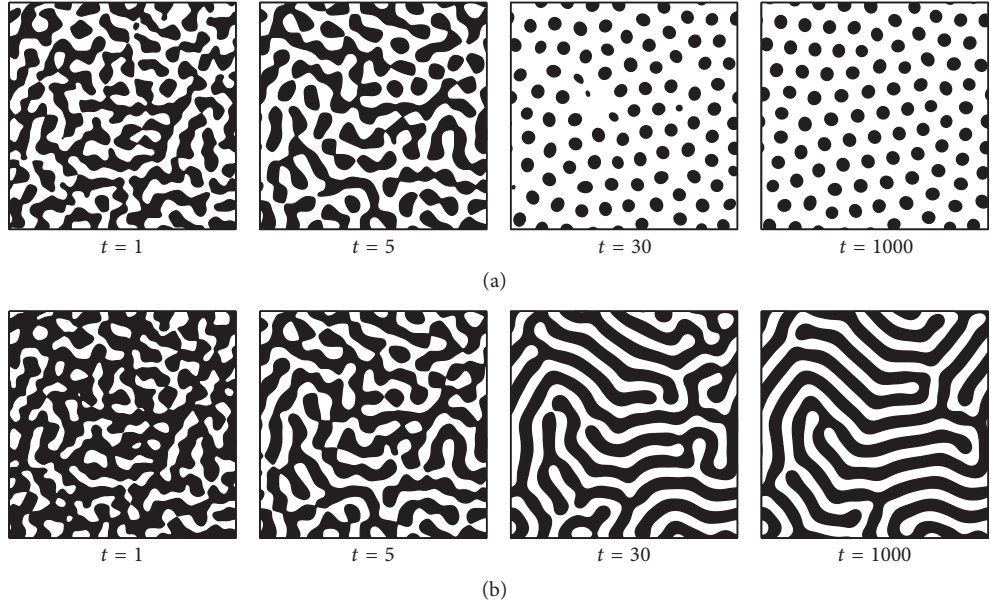


FIGURE 3: (a) Hexagonal pattern when $\bar{\phi} = -0.3$ and (b) lamella pattern when $\bar{\phi} = 0$ with $h = 0.03$, $\Delta t = 0.1$, $\alpha = 100$, $\epsilon = 0.035$, and 128×128 mesh grid. Times are shown below each column.

4. Image Inpainting

Image inpainting is the filling in of damaged or missing regions of an image with the use of information from surrounding areas [7]. In [7], authors modified the CH equation to achieve fast inpainting of a binary image. Let $f(\mathbf{x})$, where $\mathbf{x} = (x, y)$, be a given binary image in a domain Ω and $D \subset \Omega$ be the inpainting domain. The image is scaled so that

$0 \leq f \leq 1$. Let $c(\mathbf{x}, t)$ be a phase-field which is governed by the following modified CH equation:

$$\begin{aligned} c_t(\mathbf{x}, t) &= \Delta\mu(\mathbf{x}, t) + \lambda(\mathbf{x})(f(\mathbf{x}) - c(\mathbf{x}, t)), \\ \mathbf{x} \in \Omega, t > 0, \quad (6) \\ \mu(\mathbf{x}, t) &= F'(c(\mathbf{x}, t)) - \epsilon^2 \Delta c(\mathbf{x}, t), \end{aligned}$$

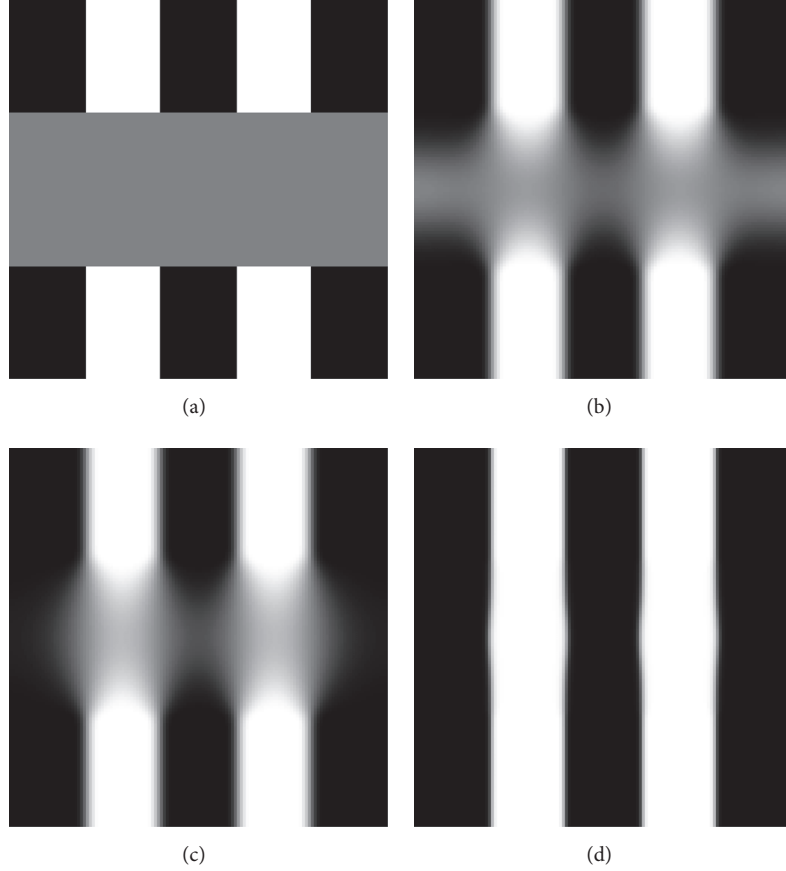


FIGURE 4: (a) Initial data with inpainting region in gray. (b), (c), and (d) are numerical solutions at $t = 40, 500$, and 1300 , respectively.

where $F(c) = 0.25c^2(1 - c)^2$ and $\lambda(\mathbf{x}) = 0$ if $\mathbf{x} \in D$; otherwise $\lambda(\mathbf{x}) = \lambda_0$.

We perform a test of the inpainting of a double stripe as shown in Figure 4(a). Here, gray region in the initial configuration denotes the inpainting region. In this test, we start the numerical test with the following parameters: $\lambda_0 = 10$, $\epsilon = 10$, $h = 1/128$, and $\Delta t = 0.1$. And then we switch these values to $\lambda_0 = 0.1$, $\epsilon = 0.1$, and $\Delta t = 1$ after 3000 iterations and stop the simulation after 4000 iterations. Figures 4(b), 4(c), and 4(d) are numerical solutions at $t = 40, 500$, and 1300 , respectively. The final inpainting result represents the completed stripe. Numerical solution algorithms can be found in [7, 30].

5. Two-Phase Fluid Flows

In the two-phase fluid flow problem, we use the CH equation for capturing the interface location between two immiscible fluids. The CH equation provides a good mass conservation property. We model the variable quantities such as viscosity and density by using the phase-field. Also, we model the surface tension effect with the phase-field. The velocity field is governed by the modified Navier–Stokes equation. The

phase-field is advected by the bulk velocity. A typical coupled model is

$$\begin{aligned} \rho(\phi) \left(\frac{\partial \mathbf{u}}{\partial t} + \mathbf{u} \cdot \nabla \mathbf{u} \right) &= -\nabla p + \frac{1}{\text{Re}} \Delta \mathbf{u} + \frac{1}{\text{We}} \mathbf{SF} \\ &\quad + \frac{\rho(\phi)}{\text{Fr}} \mathbf{g}, \\ \nabla \cdot \mathbf{u} &= 0, \\ \frac{\partial \phi}{\partial t} + \nabla \cdot (\phi \mathbf{u}) &= \frac{1}{\text{Pe}} \nabla \cdot (M(\phi) \nabla \mu), \\ \mu &= F'(\phi) - C \Delta \phi, \end{aligned} \tag{7}$$

where \mathbf{u} is the velocity, p is the pressure, $\rho(\phi)$ is the density, \mathbf{SF} is the surface tension force, \mathbf{g} is the gravitational force, ϕ is the phase-field function, $M(\phi)$ is the mobility function, and μ is the chemical potential. The dimensionless parameters are used as Reynolds number $\text{Re} = \rho_* L_* V_*/\eta_*$, Weber number $\text{We} = \rho_* L_* V_*^2/\sigma$, Froude number $\text{Fr} = V_*^2/(gL_*)$, Cahn number ϵ^2/μ_* , and diffusional Peclet number $\text{Pe} = L_* V_*/(M_* \mu_*)$, where V_* is the characteristic velocity, L_* is the characteristic length, η is the viscosity, σ is the surface tension coefficient, g is the gravitational constant, ϵ is the interfacial parameter, and

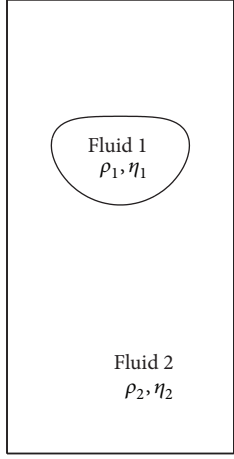


FIGURE 5: Schematic diagram of a two-phase fluid domain.

subscript * denotes the corresponding characteristic values. See [8, 31, 32] for numerical solution algorithms.

As a test problem, we consider a drop falling test under the gravity. A schematic diagram of a two-phase domain is shown in Figure 5. Figure 6 shows the interfaces of the falling drop at time $t = 0, 1, 2$, and 2.7 from left to right. The simulation is performed on the domain $\Omega = (0, 1) \times (0, 2)$ with a 128×256 mesh grid. The temporal and spatial step sizes are $\Delta t = 0.0005$ and $h = 1/128$, respectively. We use $\epsilon = 0.00151$, $\rho_1/\rho_2 = 3$, $Re = 100$, $We = 12.5$, and $Fr = 1$. Also, the radius of the initial circle is set to 0.25 .

6. Microstructure with Elastic Inhomogeneity

Strain energy stored by the elastic deformation of the object is called the elastic strain energy. This energy performs an important function in determining the transformation path and the corresponding microstructure evolution [12]. Chen and Khachaturyan [33] and Wang et al. [34] have first derived the phase-field model from the microscopic theory of Khachaturyan [35, 36]. The standard phase-field model is combined with the microelasticity theory that allows us to express the elastic energy as a function of composition and order parameters [37]. This model has been applied to a variety of solid-state phase transformations [37, 38] and used to investigate the effect of elastic strain energy on the morphological evolution of the microstructure. For more details, see [12].

Now, we derive the phase-field model for microstructural evolution. Let us consider a two-phase microstructure with a composition field $c(\mathbf{x})$ and elastic strain $\epsilon_{ij}^{\text{el}}(\mathbf{x})$. The total free energy in an inhomogeneous system is defined as

$$\mathcal{F} = \int_V \left[F(c) + \mathcal{E}_{\text{el}} + \frac{\kappa}{2} |\nabla c|^2 \right] dV. \quad (8)$$

Here, $F(c)$ is the local chemical free energy density defined by a quartic polynomial $F(c) = 2.5(c - c^\alpha)^2(c - c^\beta)^2$ with two local minima c^α and c^β . Assuming that materials are

cubic anisotropy, the elastic strain energy density $\mathcal{E}_{\text{el}}(c, \mathbf{u})$ is defined as

$$\begin{aligned} \mathcal{E}_{\text{el}}(c, \mathbf{u}) = & -(C_{11} + C_{12}) e(c) (E_{11} + E_{22} - e(c)) \\ & + 2C_{44}E_{12}^2 + 0.5C_{11}(E_{11}^2 + E_{22}^2) \\ & + C_{12}E_{11}E_{22}, \end{aligned} \quad (9)$$

where $\mathbf{u} = (u, v)$ is the displacement and C_{11} , C_{12} , and C_{44} are the cubic elastic parameters and are dependent on the order parameter c . Here, $C_k = C_k^1 c + C_k^0(1 - c)$ for $k = 11, 12$, and 44 , where C_k^0 and C_k^1 are elastic constants of matrix and precipitate, respectively. The eigenstrain is $e(c) = \eta(c - c_s)$, which obeys Vegard's law. Here, c_s is the average composition and η is a constant. And $E_{11} = u_x$, $E_{22} = v_y$, and $E_{12} = 0.5(u_y + v_x)$. κ is the gradient energy coefficient which can be related to interatomic interaction parameters. By the variational derivative $\delta\mathcal{F}/\delta c$, we obtain the following equation:

$$\frac{\partial \mathcal{F}}{\partial c} = F'(c) - \kappa\Delta c + \frac{\partial \mathcal{E}_{\text{el}}}{\partial c}. \quad (10)$$

From the total free energy functional (8), we derive the modified CH equation for the two-dimensional microstructure evolution with strong elastic inhomogeneity:

$$\begin{aligned} \frac{\partial c}{\partial t} &= M\Delta\mu, \\ \mu &= F'(c) - \epsilon^2\Delta c + \frac{\partial \mathcal{E}_{\text{el}}}{\partial c}, \end{aligned} \quad (11)$$

where M is the mobility. From the definition, we get

$$\begin{aligned} \frac{\partial \mathcal{E}_{\text{el}}}{\partial c} &= - (C_{11}^1 - C_{11}^0 + C_{12}^1 - C_{12}^0) e(c) (E_{11} + E_{22} - e(c)) \\ & - \eta(C_{11} + C_{12})(E_{11} + E_{22} - 2e(c)) \\ & + 2(C_{44}^1 - C_{44}^0) E_{12}^2 \\ & + 0.5(C_{11}^1 - C_{11}^0)(E_{11}^2 + E_{22}^2) \\ & + (C_{12}^1 - C_{12}^0) E_{11}E_{22}. \end{aligned} \quad (12)$$

Under the condition for plain strain and the quasi-static approximation, we have

$$\begin{aligned} & (C_{11}u_x + C_{12}v_y)_x + (C_{44}u_y + C_{44}v_x)_y \\ & = [(C_{11} + C_{12})e(c)]_x, \\ & (C_{11}v_y + C_{12}u_x)_y + (C_{44}v_x + C_{44}u_y)_x \\ & = [(C_{11} + C_{12})e(c)]_y, \end{aligned} \quad (13)$$

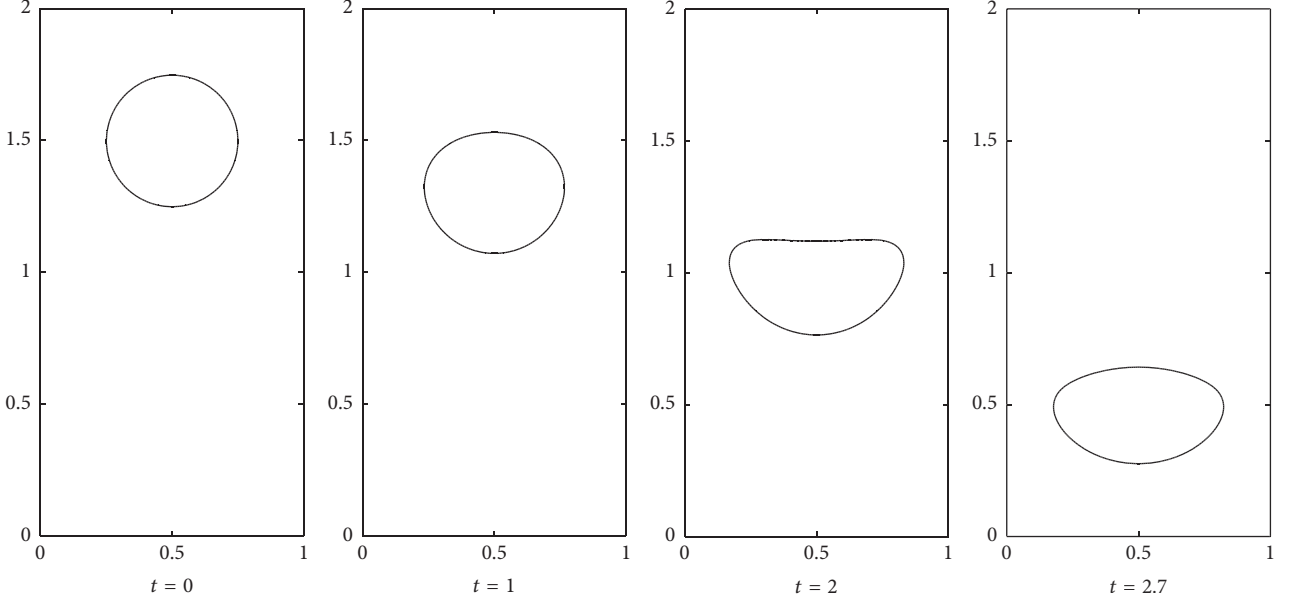


FIGURE 6: Evolution of falling drop shapes with $\rho_1/\rho_2 = 3$, $Re = 100$, $We = 12.5$, and $Fr = 1$. Times are shown below in each figure.

where the subscripts x and y denote partial derivatives with respect to the corresponding arguments.

Now, we perform a numerical test with $\kappa = 1.2247$, $c^\alpha = 0.053$, $c^\beta = 0.947$, the composition expansion coefficient $\eta = 0.05$, spatial step size $h = 1$, temporal step size $\Delta t = 1$, and the computational domain $\Omega = (0, 256) \times (0, 256)$. With an initial condition,

$$\begin{aligned} c(x, y, 0) \\ = \begin{cases} 0.947, & \text{if } \sqrt{(x - 128)^2 + (y - 128)^2} \leq 40 \\ 0.060, & \text{otherwise,} \end{cases} \end{aligned} \quad (14)$$

we investigate the effect of elastic inhomogeneity κ . We take the elastic constants $C_{11}^0 = 232$, $C_{12}^0 = 153$, and $C_{44}^0 = 117$ in the same values in [39, 40], which have a cubically anisotropic system. In order to show the effect of elastic inhomogeneity, we keep the same bulk modulus $B = C_{11} + C_{12}$ and the same ratio of anisotropy $\delta = 2C_{44}/(C_{11} - C_{12})$, while changing the ratio of shear modulus $\kappa = C_{44}^P/C_{44}^M$ in the matrix and precipitate phases, respectively [39].

Figures 7(a)–7(f) show the numerical results at time $t = 1700$ with the ratio of shear modulus $\kappa = 1.7, 1.35, 1, 0.6, 0.45$, and 0.3 , respectively. The decrease of κ means that $C_{44}^P = \kappa C_{44}^M$; that is, the stiffness of the precipitate is less than the matrix [41–43]. Therefore, the precipitate phase is easy to deform to star shape when $\kappa < 1$ as shown in Figures 7(e) and 7(f). For a comparison study of the effect of free energies (polynomial and logarithmic functions) on the dynamics, see [44].

7. Tumor Growth Simulation

To provide optimal strategies for treatments, a mathematical modeling is very useful since it gives systematic investigation. Let Ω be a computational domain. Let Ω_H , Ω_V , and Ω_D be the healthy, viable, and dead tumor tissues, respectively. We also define $\Omega_T = \Omega_V \cup \Omega_D$ as the tumor cell. See Figure 8 for the schematic of these definitions.

Let ϕ_T and ϕ_D be the volume fractions of tumor and dead tumor tissues. Then, the nondimensional equations for the volume fraction of tumor cells are

$$\begin{aligned} \frac{\partial \phi_T}{\partial t} &= M \nabla \cdot (\phi_T \nabla \mu) + S_T - \nabla \cdot (\phi_T \mathbf{u}_S), \\ \mu &= F'(\phi_T) - \epsilon^2 \Delta \phi_T, \end{aligned} \quad (15)$$

$$S_T = nG(\phi_T)(\phi_T - \phi_D) - \lambda_L \phi_D,$$

where $G(\phi_T)$ is a continuous cut-off function. The nondimensional equations for the volume fraction of necrotic cells are

$$\frac{\partial \phi_D}{\partial t} = M \nabla \cdot (\phi_D \nabla \mu) + S_D - \nabla \cdot (\phi_D \mathbf{u}_S), \quad (16)$$

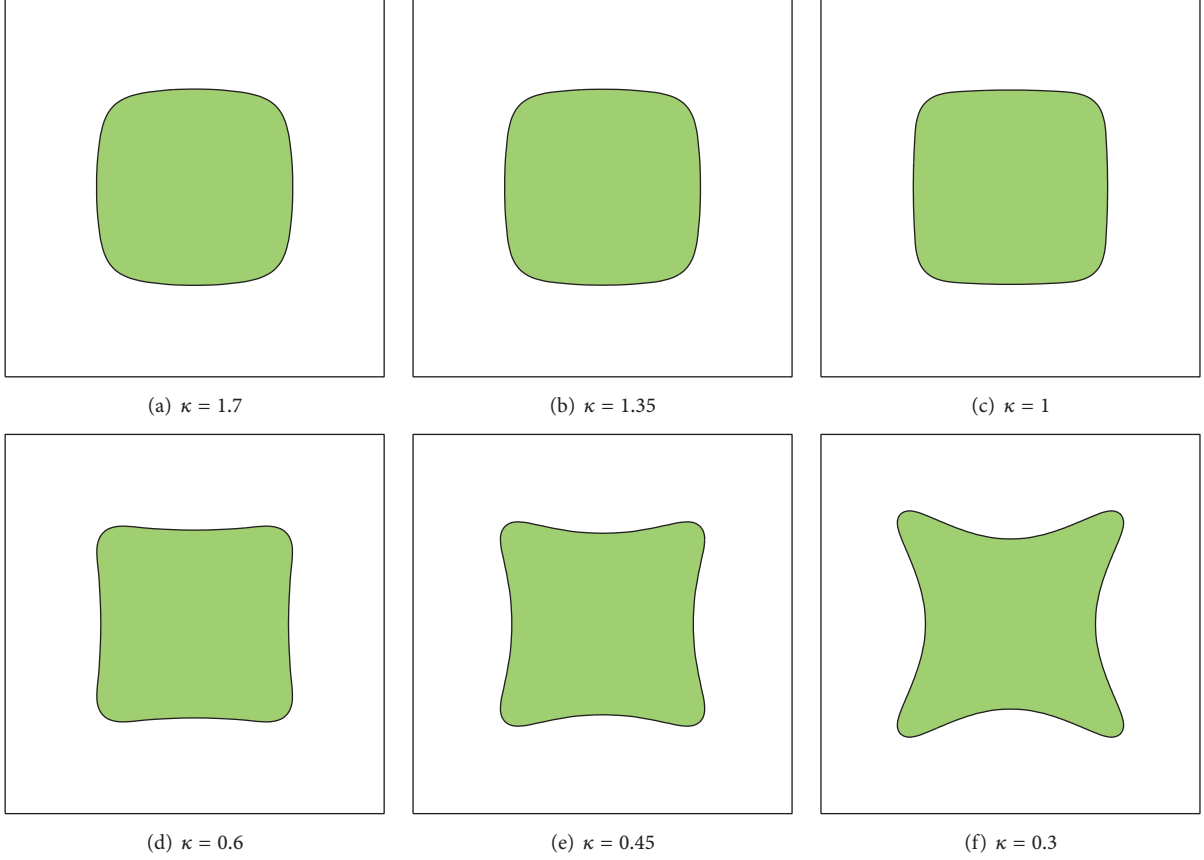
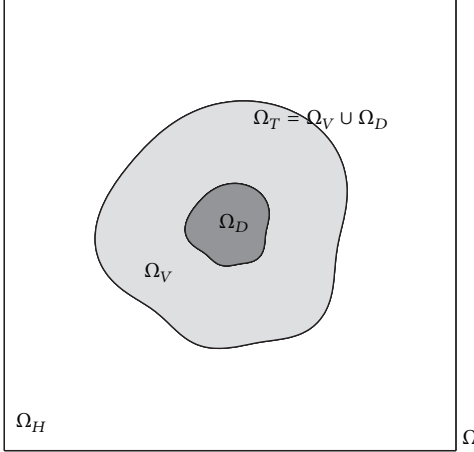
$$S_D = (\lambda_A + \lambda_N \mathcal{H}(n_N - n))(\phi_T - \phi_D) - \lambda_L \phi_D,$$

where \mathcal{H} is the Heaviside function. The nondimensional cell velocity is

$$\mathbf{u} = -\kappa(\phi_T, \phi_D) \left(\nabla p - \frac{\gamma}{\epsilon} \mu \nabla \phi_T \right), \quad (17)$$

where γ is a nondimensional measure of the adhesion force. The velocity satisfies

$$\nabla \cdot \mathbf{u} = S_T. \quad (18)$$

FIGURE 7: Morphologies of a circular precipitate with different shear modulus κ at time $t = 1700$.FIGURE 8: Schematic of the domain for tumor simulation. Ω , Ω_H , Ω_V , Ω_D , and Ω_T are the computational domain, healthy cell, viable cell, dead cell, and tumor, respectively.

The nondimensional quasi-steady nutrient equation is

$$0 = \nabla \cdot (D(\phi_T) \nabla n) + T_c(\phi_T, n) - n(\phi_T - \phi_D), \quad (19)$$

where the diffusion coefficient and nutrient capillary source term are

$$\begin{aligned} D(\phi_T) &= D_H(1 - Q(\phi_T)) + Q(\phi_T), \\ T_C(\phi_T, n) &= (\gamma_P^H(1 - Q(\phi_T)) + \gamma_P^T Q(\phi_T))(n_C - n), \end{aligned} \quad (20)$$

where D_H is the nutrient diffusivity in the healthy tissue and $Q(\phi_T)$ is an interpolation function. For more details about the functions and parameters, see [17]. Also, numerical simulation using phase-field method can be found in [45–47].

Figures 9(a)–9(c) show the numerical results at times $t = 0$, $t = 50$, and $t = 100$, respectively [17]. The parameters are $\gamma_P^H = 0.5$, $n_C = 1$, $D_H = 1$, $\lambda_A = 0$, $\lambda_L = 1$, $M = 10$, $\gamma_P^T = 0$, $\kappa = 1$, $n_N = 0.4$, $\lambda_N = 3$, $\gamma = 0$, and $\epsilon = 0.1$.

8. Topology Optimization

Zhou and Wang [16] extended the phase-field approach to the problem of minimizing the mean compliance of a multimaterial structure. For a four-phase system, we have

$$\begin{aligned} \frac{\partial c}{\partial t} &= \nabla \cdot (M(c) \nabla \mu), \\ \mu &= F'(c) - \Gamma_\epsilon \Delta c + w(c), \end{aligned} \quad (21)$$

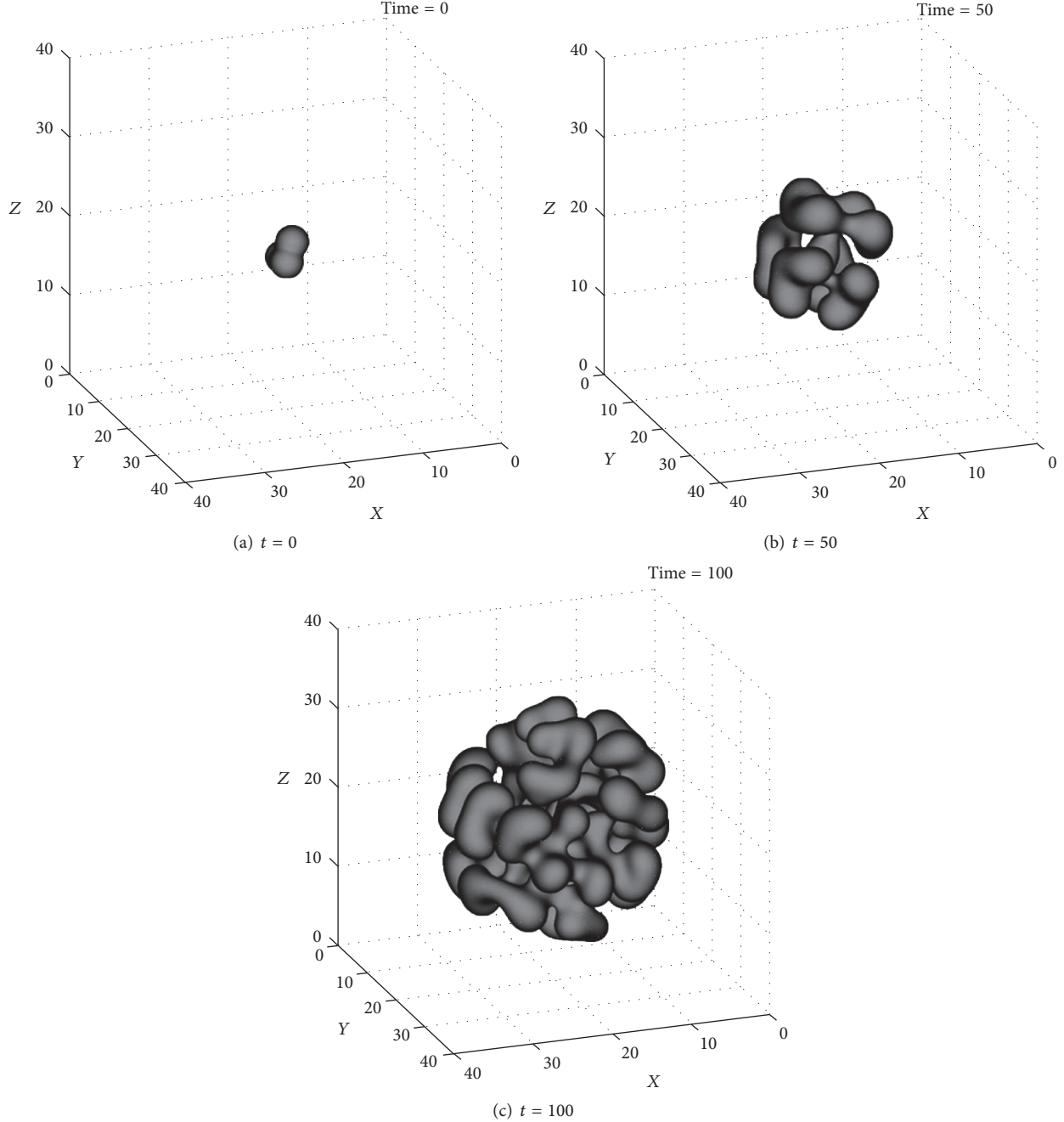


FIGURE 9: Evolution of the $\phi_T = 0.5$ isosurface during the growth of an asymmetrical 3D tumor (reprinted from Wise et al. [17], with permission from Elsevier).

where

$$c = \begin{pmatrix} \alpha \\ \beta \\ \gamma \end{pmatrix},$$

$$\mu = \begin{pmatrix} \xi \\ \zeta \\ \psi \end{pmatrix},$$

$$\Gamma_\epsilon = \begin{pmatrix} 2\epsilon^2 & \epsilon^2 & \epsilon^2 \\ \epsilon^2 & 2\epsilon^2 & \epsilon^2 \\ \epsilon^2 & \epsilon^2 & 2\epsilon^2 \end{pmatrix},$$

$$f(c) = \begin{pmatrix} \frac{\partial F}{\partial \alpha} \\ \frac{\partial F}{\partial \beta} \\ \frac{\partial F}{\partial \gamma} \end{pmatrix},$$

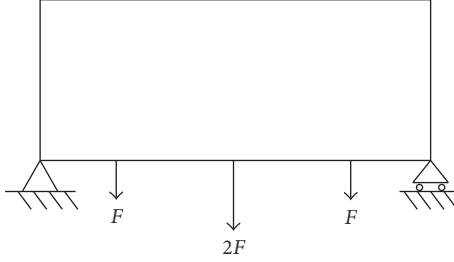
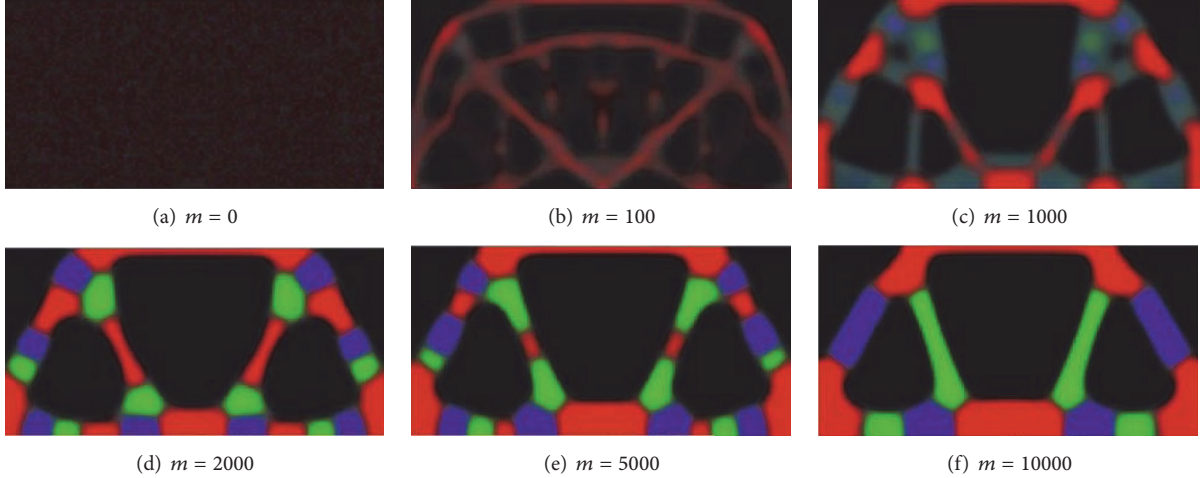


FIGURE 10: Design domain of topology optimization.

FIGURE 11: Solution results for the four-material bridge structure at given time steps m : material 1 in green (softest), material 2 (softer) in blue, material 3 (hardest) in red, and the void in black (reprinted from Zhou and Wang [16], with permission from Springer).

$$w(c) = \begin{pmatrix} \frac{\partial W^*}{\partial \alpha} \\ \frac{\partial W^*}{\partial \beta} \\ \frac{\partial W^*}{\partial \gamma} \end{pmatrix}. \quad (22)$$

The bulk energy is defined as

$$F(c) = \kappa [\alpha^2 (\beta^2 + \gamma^2 + \nu^2) + \beta^2 (\gamma^2 + \nu^2) + \gamma^2 \nu^2 + \alpha^2 \beta^2 (\gamma^2 + \nu^2) + \beta^2 \gamma^2 \nu^2], \quad (23)$$

where $\nu = 1 - \alpha - \beta - \gamma$ is the fourth phase and κ is a constant. Here, $W^*(u(c))$ is defined as

$$W^*(u(c)) = \frac{1}{2} \int_{\Omega} \epsilon_{ij}(u) : E_{ijkl}(c) \epsilon_{kl}(u) d\Omega. \quad (24)$$

More details about the modeling and simulation can be found in [16].

Figure 10 shows a schematic of a bridge structure. The design domain has a length to height ratio of 2:1. The left bottom corner is fixed while the right bottom corner is simply supported.

Figure 11 shows the system changes from a random initial mix to a final optimal bridge structure. The volume ratio for the three hard material phases is 0.1:0.1:0.2 and the ratio of Young's modulus is 1:3:9. $\Delta t = 0.1h$, $\eta = 0.05$, and $\epsilon = 0.005$ are used. The FEM mesh is of 64×64 quadrilateral elements.

9. Conclusions

In this article, we reviewed and described the basic mechanism of the phase-field modeling with the CH equation. It is important to understand the fundamental dynamics of the CH equation in various models since we can use it to model physical phenomena involving deformable interfaces. As a future work, it would be interesting to review the multicomponent CH equation.

Competing Interests

The authors declare that there is no conflict of interests regarding the publication of this paper.

Acknowledgments

Seok-Min Lee was supported by the Hongik University new faculty research support fund.

References

- [1] J. W. Cahn, "On spinodal decomposition," *Acta Metallurgica*, vol. 9, no. 9, pp. 795–801, 1961.
- [2] J. W. Cahn and J. E. Hilliard, "Free energy of a nonuniform system. I. Interfacial free energy," *The Journal of Chemical Physics*, vol. 28, no. 2, pp. 258–267, 1958.
- [3] M. Maraldi, L. Molari, and D. Grandi, "A unified thermodynamic framework for the modelling of diffusive and displacive phase transitions," *International Journal of Engineering Science*, vol. 50, no. 1, pp. 31–45, 2012.
- [4] R. Choksi, M. A. Peletier, and J. F. Williams, "On the phase diagram for microphase separation of diblock copolymers: an approach via a nonlocal Cahn-Hilliard functional," *SIAM Journal on Applied Mathematics*, vol. 69, no. 6, pp. 1712–1738, 2009.
- [5] D. Jeong, S. Lee, Y. Choi, and J. Kim, "Energy-minimizing wavelengths of equilibrium states for diblock copolymers in the hex-cylinder phase," *Current Applied Physics*, vol. 15, no. 7, pp. 799–804, 2015.
- [6] D. Jeong, J. Shin, Y. Li et al., "Numerical analysis of energy-minimizing wavelengths of equilibrium states for diblock copolymers," *Current Applied Physics*, vol. 14, no. 9, pp. 1263–1272, 2014.
- [7] A. L. Bertozzi, S. Esedoglu, and A. Gillette, "Inpainting of binary images using the Cahn-Hilliard equation," *IEEE Transactions on Image Processing*, vol. 16, no. 1, pp. 285–291, 2007.
- [8] V. E. Badalassi, H. D. Ceniceros, and S. Banerjee, "Computation of multiphase systems with phase field models," *Journal of Computational Physics*, vol. 190, no. 2, pp. 371–397, 2003.
- [9] M. Heida, "On the derivation of thermodynamically consistent boundary conditions for the Cahn–Hilliard–Navier–Stokes system," *International Journal of Engineering Science*, vol. 62, pp. 126–156, 2013.
- [10] M. Kotschote and R. Zacher, "Strong solutions in the dynamical theory of compressible fluid mixtures," *Mathematical Models and Methods in Applied Sciences*, vol. 25, no. 7, pp. 1217–1256, 2015.
- [11] M. Asle Zaeem, H. El Kadiri, M. F. Horstemeyer, M. Khafizov, and Z. Utlegulov, "Effects of internal stresses and intermediate phases on the coarsening of coherent precipitates: a phase-field study," *Current Applied Physics*, vol. 12, no. 2, pp. 570–580, 2012.
- [12] J. Zhu, L.-Q. Chen, and J. Shen, "Morphological evolution during phase separation and coarsening with strong inhomogeneous elasticity," *Modelling and Simulation in Materials Science and Engineering*, vol. 9, no. 6, pp. 499–511, 2001.
- [13] D. Hilhorst, J. Kampmann, T. Nguyen, and K. G. Van Der Zee, "Formal asymptotic limit of a diffuse-interface tumor-growth model," *Mathematical Models and Methods in Applied Sciences*, vol. 25, no. 6, pp. 1011–1043, 2015.
- [14] S. M. Wise, J. S. Lowengrub, H. B. Frieboes, and V. Cristini, "Three-dimensional multispecies nonlinear tumor growth? I: model and numerical method," *Journal of Theoretical Biology*, vol. 253, no. 3, pp. 524–543, 2008.
- [15] M. H. Farshbaf-Shaker and C. Heinemann, "A phase field approach for optimal boundary control of damage processes in two-dimensional viscoelastic media," *Mathematical Models and Methods in Applied Sciences*, vol. 25, no. 14, pp. 2749–2793, 2015.
- [16] S. Zhou and M. Y. Wang, "Multimaterial structural topology optimization with a generalized Cahn–Hilliard model of multiphase transition," *Structural and Multidisciplinary Optimization*, vol. 33, no. 2, pp. 89–111, 2007.
- [17] S. M. Wise, J. S. Lowengrub, and V. Cristini, "An adaptive multigrid algorithm for simulating solid tumor growth using mixture models," *Mathematical and Computer Modelling*, vol. 53, no. 1-2, pp. 1–20, 2011.
- [18] D. Lee, J.-Y. Huh, D. Jeong, J. Shin, A. Yun, and J. Kim, "Physical, mathematical, and numerical derivations of the Cahn–Hilliard equation," *Computational Materials Science*, vol. 81, pp. 216–225, 2014.
- [19] S.-D. Yang, H. G. Lee, and J. Kim, "A phase-field approach for minimizing the area of triply periodic surfaces with volume constraint," *Computer Physics Communications*, vol. 181, no. 6, pp. 1037–1046, 2010.
- [20] L. Cherfils and M. Petcu, "A numerical analysis of the Cahn–Hilliard equation with non-permeable walls," *Numerische Mathematik*, vol. 128, no. 3, pp. 517–549, 2014.
- [21] A. Christlieb, K. Promislow, and Z. Xu, "On the unconditionally gradient stable scheme for the Cahn–Hilliard equation and its implementation with Fourier method," *Communications in Mathematical Sciences*, vol. 11, no. 2, pp. 345–360, 2013.
- [22] M. Fernandino and C. A. Dorao, "The least squares spectral element method for the Cahn–Hilliard equation," *Applied Mathematical Modelling*, vol. 35, no. 2, pp. 797–806, 2011.
- [23] M. Hintermüller, M. Hinze, and M. H. Tber, "An adaptive finite-element Moreau–Yosida-based solver for a non-smooth Cahn–Hilliard problem," *Optimization Methods and Software*, vol. 26, no. 4–5, pp. 777–811, 2011.
- [24] N. Lecoq, H. Zapsolsky, and P. Galenko, "Numerical approximation of the Cahn–Hilliard equation with memory effects in the dynamics of phase separation," *Discrete and Continuous Dynamical Systems A*, vol. 31, pp. 953–962, 2011.
- [25] S. Lezama-Alvarez, E. O. Avila-Davila, V. M. Lopez-Hirata, and J. L. Gonzalez-Velazquez, "Numerical analysis of phase decomposition in A-B binary alloys using Cahn–Hilliard equations," *Materials Research*, vol. 16, no. 5, pp. 975–981, 2013.
- [26] G. Tierra and F. Guillén-González, "Numerical methods for solving the Cahn–Hilliard equation and its applicability to related energy-based models," *Archives of Computational Methods in Engineering*, vol. 22, no. 2, pp. 269–289, 2015.
- [27] O. Wodo and B. Ganapathysubramanian, "Computationally efficient solution to the Cahn–Hilliard equation: adaptive implicit time schemes, mesh sensitivity analysis and the 3D isoperimetric problem," *Journal of Computational Physics*, vol. 230, no. 15, pp. 6037–6060, 2011.
- [28] T. Ohta and K. Kawasaki, "Equilibrium morphology of block copolymer melts," *Macromolecules*, vol. 19, no. 10, pp. 2621–2632, 1986.
- [29] I. Ohnishi, Y. Nishiura, M. Imai, and Y. Matsushita, "Analytical solutions describing the phase separation driven by a free energy functional containing a long-range interaction term," *Chaos*, vol. 9, no. 2, pp. 329–341, 1999.
- [30] D. Jeong, Y. Li, H. G. Lee, and J. Kim, "Fast and automatic inpainting of binary images using a phase-field model," *Journal of the Korean Society for Industrial and Applied Mathematics*, vol. 13, no. 3, pp. 225–236, 2009.
- [31] X. Feng, "Fully discrete finite element approximations of the Navier–Stokes–Cahn–Hilliard diffuse interface model for two-phase fluid flows," *SIAM Journal on Numerical Analysis*, vol. 44, no. 3, pp. 1049–1072, 2006.
- [32] J. Kim, "A continuous surface tension force formulation for diffuse-interface models," *Journal of Computational Physics*, vol. 204, no. 2, pp. 784–804, 2005.

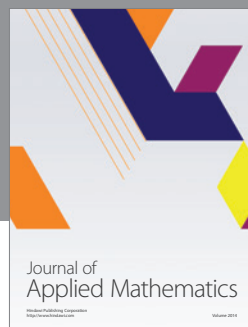
- [33] L.-Q. Chen and A. G. Khachaturyan, "Computer simulation of structural transformations during precipitation of an ordered intermetallic phase," *Acta Metallurgica et Materialia*, vol. 39, no. 11, pp. 2533–2551, 1991.
- [34] Y. Wang, L.-Q. Chen, and A. G. Khachaturyan, "Kinetics of strain-induced morphological transformation in cubic alloys with a miscibility gap," *Acta Metallurgica Et Materialia*, vol. 41, no. 1, pp. 279–296, 1993.
- [35] A. G. Khachaturyan, "Microscopic theory of diffusion in crystalline solid solutions and the time evolution of the diffuse scattering of X rays and thermal neutrons," *Soviet Physics Solid State, USSR*, vol. 9, no. 9, pp. 2040–2046, 1968.
- [36] A. G. Khachaturyan, *Theory of Structural Transformations in Solids*, Wiley-Interscience, New York, NY, USA, 1985.
- [37] N. Moelans, B. Blanpain, and P. Wollants, "An introduction to phase-field modeling of microstructure evolution," *Calphad*, vol. 32, no. 2, pp. 268–294, 2008.
- [38] L.-Q. Chen, "Phase-field models for microstructure evolution," *Annual Review of Materials Science*, vol. 32, no. 1, pp. 113–140, 2002.
- [39] S. Y. Hu and L. Q. Chen, "A phase-field model for evolving microstructures with strong elastic inhomogeneity," *Acta Materialia*, vol. 49, no. 11, pp. 1879–1890, 2001.
- [40] O. Paris, F. Langmyar, G. Vogl, and P. Fratzl, "Possible criterion for slowing down of precipitate coarsening due to elastic misfit interactions," *Zeitschrift für Metallkunde*, vol. 86, no. 12, pp. 860–863, 1995.
- [41] J. K. Lee, "A study on coherency strain and precipitate morphology via a discrete atom method," *Metallurgical and Materials Transactions A: Physical Metallurgy and Materials Science*, vol. 27, no. 6, pp. 1449–1459, 1996.
- [42] J. K. Lee, "Elastic stress and microstructural evolution," *Materials Transactions, JIM*, vol. 39, no. 1, pp. 114–132, 1998.
- [43] I. Schmidt, R. Mueller, and D. Gross, "The effect of elastic inhomogeneity on equilibrium and stability of a two particle morphology," *Mechanics of Materials*, vol. 30, no. 3, pp. 181–196, 1998.
- [44] D. Jeong, S. Lee, and J. Kim, "An efficient numerical method for evolving microstructures with strong elastic inhomogeneity," *Modelling and Simulation in Materials Science and Engineering*, vol. 23, no. 4, Article ID 045007, 2015.
- [45] V. Cristini, H. B. Frieboes, X. Li et al., "Nonlinear modeling and simulation of tumor growth," in *Selected Topics in Cancer Modeling*, pp. 113–181, Birkhauser, Boston, Mass, USA, 2008.
- [46] V. Cristini and J. Lowengrub, *Multiscale Modeling of Cancer: An Integrated Experimental and Mathematical Modeling Approach*, Cambridge University Press, 2010.
- [47] R. D. M. Travasso, M. Castro, and J. C. R. E. Oliveira, "The phase-field model in tumor growth," *Philosophical Magazine*, vol. 91, no. 1, pp. 183–206, 2011.



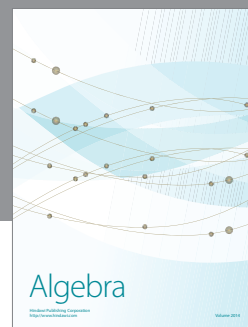
Advances in
Operations Research



Advances in
Decision Sciences



Journal of
Applied Mathematics



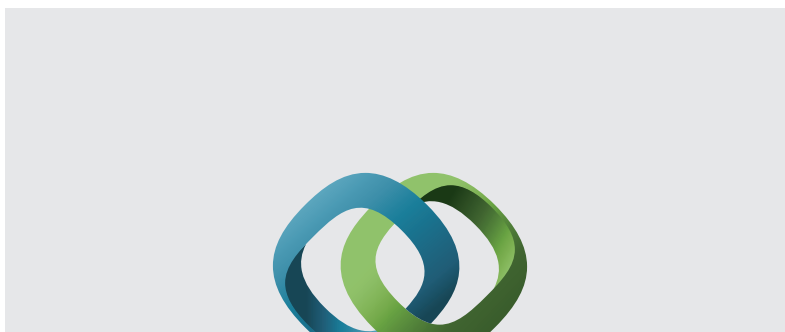
Algebra



Journal of
Probability and Statistics



The Scientific
World Journal

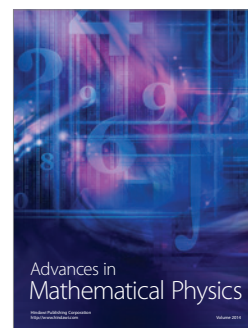


Hindawi

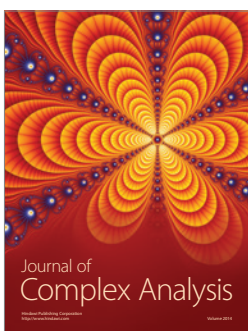
Submit your manuscripts at
<http://www.hindawi.com>



International Journal of
Combinatorics



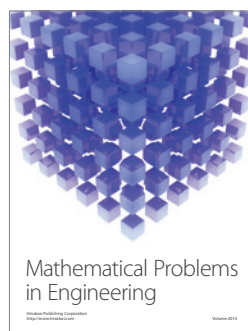
Advances in
Mathematical Physics



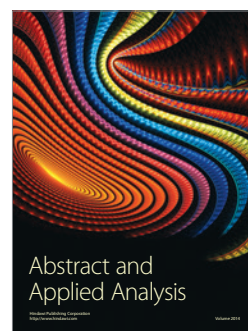
Journal of
Complex Analysis



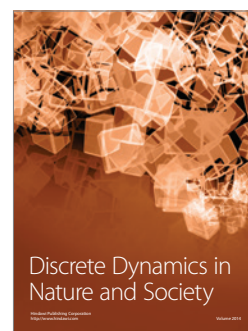
Journal of
Mathematics



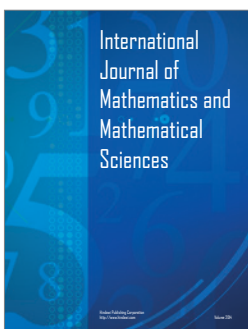
Mathematical Problems
in Engineering



Abstract and
Applied Analysis



Discrete Dynamics in
Nature and Society



International
Journal of
Mathematics and
Mathematical
Sciences



Journal of
Discrete Mathematics



Journal of
Function Spaces



International Journal of
Stochastic Analysis



Journal of
Optimization